ANTIOXIDANTS & REDOX SIGNALING
Volume 16, Number 5, 2012

DOI: 10.1089/ars.2011.4103

ORIGINAL RESEARCH COMMUNICATION

Reactive Oxygen Species-Mediated p53 Core-Domain Modifications Determine Apoptotic or Necrotic Death in Cancer Cells

Rajan Gogna,[1,*] Esha Madan,[1,*] Periannan Kuppusamy,[2] and Uttam Pati[1]

Abstract

Aims: *p53* is known to induce apoptotic and necrotic cell death in response to stress, although the mechanism of these pathways is unknown. The aim of this study was to determine the molecular mechanism that determines *p53*'s decision to select the apoptotic or necrotic mode of cell death. ***Results:*** Gold nanoparticles (Au-NPs) induced both apoptosis and necrosis in cancer cells in a *p53*-dependent manner. In cells undergoing apoptosis and necrosis, differential patterns of reactive oxygen species (ROS) generation were observed that leads to the activation of two different sets of p53-interacting kinases and acetylases. The differential activation of cellular kinases and acetylases caused dissimilar patterns of p53 phosphorylation and acetylation. In apoptotic cells, p53 was post-translationally modified in the core-domain, whereas in necrotic cells, it was modified at both N- and C-terminii, thus displaying differential DNA-binding activity. Au-NP10 and Au-NP80 activated fifty apoptotic and fifty nine necrotic p53-downstream genes, respectively. Both Au-NP10 and Au-NP80 showed HCT (p53+/+) tumor regression in mice xenografts. ***Innovation:*** This study established for the first time that, in cancer cells, Au-NP-mediated apoptosis and necrosis are controlled by differential activation of *p53* and its downstream genes. Further, both Au-NP10 and Au-NP80 were shown to regress HCT (p53+/+) tumors *via* apoptotic and necrotic pathways, respectively. ***Conclusion:*** Au-NP-mediated *p53* activation at both transcription and proteome level, through ROS-mediated p53 post-translational modification pattern, is responsible for tumor regression, which may further find wider application of nanoparticles in cancer therapy. *Antioxid. Redox Signal.* 16, 400–412.

Introduction

The cell in response to the density of death stimulus may undergo apoptosis or necrosis (47, 49). The role of *p53* in the mitochondrion-dependent apoptotic program has been well studied (45); its role in the necrotic signaling pathway is unknown. Recently, it was shown that a *p53*-initiated genetic program was responsible for programmed necrotic death *via p53-cathepsin* axis in co-operation with reactive oxygen species (ROS) (40). Cellular-stress-generated ROS and ROS-mediated responses resulted in recruitment of *p53* (21); however, the mechanism of ROS-p53 interaction has not been determined (23). Although p53 post-translational modifications might play a crucial role (44), the precise mechanism(s) of *p53* activation and its choice to evoke different cellular responses are not fully understood. Phosphorylation and acetylation, induced by multiple stress-activated kinases, are essential for p53 stabilization and activation of p53 target genes; specifically, Ser^{46} is critical for induction of apoptosis (4, 17, 20, 22, 28). p53 Ser^{392} phosphorylation regulates the sequence-specific DNA binding (13, 33), and p53 is acetylated by the human MYST family of acetyl-transferases *(hMOF, TIP60, HBO1, MOZ,* and *MORF)* in addition to other p53 interacting acetylases such as *p300, CBP, HGCNS,* and *RIP160*.

Gold nanoparticle (Au-NP) have been extensively used in cancer diagnosis (8, 9), treatment (11), and as delivery vectors for biological (7) and pharmacologic agents (27, 39). The cytotoxicity of Au-NP varied according to their sizes and in a cell-specific manner (30), and their role in cellular arrest (3), DNA damage (2), and apoptosis (26, 42) has been observed. Small- and large-size Au-NPs were recently shown to induce apoptosis and necrosis (16, 30), respectively, in cancer cells, and their mechanism of action and therapeutic applications are still unknown. Au-NP incubation in monocytes generated ROS (29), and ROS induced post-translational modification such as phosphorylation of p53 on Ser^{20} that was mediated in part by *plk-3* (46). Due to their bio-medical relevance and their

[1]Transcription and Human Biology Laboratory, School of Biotechnology, Jawaharlal Nehru University, New Delhi, India.
[2]Davis Heart and Lung Research Institute, Department of Internal Medicine, The Ohio State University, Columbus, Ohio.
*These authors contributed equally to this work.

Innovation

p53 is known to induce apoptosis and necrosis in cancer cells by transcriptionally activating its downstream genes. However, the molecular mechanism that enables *p53* to choose between these two pathways of programmed cell death is unknown. In this study, we have shown for the first time that, in cancer cells, small- (Au-NP10) and large-size (Au-NP80) nanoparticles induced apoptosis and necrosis *via* activation of p53-dependent apoptotic and necrotic gene clusters. Gold nanoparticles (Au-NPs) induced different sets of protein kinases and acetylases that differentially modified p53 in determining their DNA-binding properties. We identified that cellular reactive oxygen species level is responsible for the activation of specific sets of kinases and acetylases that could differentially modify p53. *p53* activation at both the transcription and proteome level controlled the transcription of both apoptotic and necrotic gene clusters that subjected the cancer cells to undergo apoptosis or necrosis. Further, the selective regression of tumor xenografts (HCT, p53+/+) by both Au-NPs suggested that *p53*'s decision to control tumor regression is genetically controlled. Our study highlights the molecular mechanism of how nanoparticles function *in vivo* and will add new dimensions in utilizing nanoparticles for cancer therapy.

role in diverse type cell death, it was important to determine the mechanism of action at the molecular level.

In this study, we explored the mechanism of *p53*-mediated, apoptotic, and necrotic mode of cell death in cancer cells. We hypothesized that the decision between p53-dependent apoptotic and necrotic mode of cell-death might differentially be influenced by p53 post-translational modification patterns. We have shown that small- and large-size nanoparticles increased cellular ROS that, in turn, resulted in differential p53-activation, *via* induction of different sets of p53-interacting kinases and acetylases, thus causing differential p53 post-translational modifications. The differentially activated p53 switched on fifty p53-dependent apoptotic genes in Au-NP10-treated cells and fifty-nine necrotic genes in Au-NP80-treated MCF-7 cells. Both Au-NP10 and Au-NP80 regressed HCT (p53+/+) tumor in mice xenografts. This study established that Au-NP-mediated differential *p53* activation causes tumor regression *via* apoptotic and necrotic pathways.

Results

Au-NP10 and Au-NP80 induced differential ROS and p53 *gene activation*

In response to a given death stimulus (47, 49), the cell might undergo *p53*-mediated apoptosis or necrosis, depending on the dose of the insult. Au-NPs were shown to induce cell death in cancer cells (30), although their size determined whether apoptosis or necrosis would follow (26, 42). In order to probe whether small-size Au-NP10 particles induced apoptosis and large-size Au-NP80 particles induced necrosis, we first measured their IC_{50} values in cancer cell lines carrying Wt-*p53* (MCF-7, HepG2, *p53*+/+), null-*p53* (H1299, p53−/−), and Mt-*p53* (PC3) (Fig. 1A). The results showed that both Au-NP10 and Au-NP80 were cytotoxic to cancer cells with wild-type p53. In order to establish the role of p53 in Au-NP10- and Au-NP80-mediated cytotoxicity, the IC_{50} values of the Au-NPs were determined in p53-positive and p53-deficient cell lines of the same origin. The IC_{50} values of Au-NP10 and Au-NP80 were compared between *p53*(+/+) and *p53*(−/−) variants of HCT, MCF-7, H1299, and SAOS-2 cells. The results showed that both Au-NP10 and Au-NP80 were cytotoxic only in cells with *p53* (Supplementary Fig. S1; Supplementary Data are available online at www.liebertonline.com/ars). Au-NP has been shown to induce ROS in cancer cells (29), and ROS and *p53* are known to have an inter-dependent relationship (21). ROS levels were measured in Au-NP10- and Au-NP80-treated MCF-7 cells (Fig. 1B). Au-NP10 induced twofold higher ROS (MFI-193) than Au-NP80 (MFI-98, Control cells MFI-26). These data established that Au-NP10 and Au-NP80 induced differential ROS in cancer cells with Wt-*p53*. Further, a time-course analysis (every 1 h) of ROS synthesis was conducted in Au-NP10- and Au-NP80-treated MCF-7 cells (Supplementary Fig. S2). The results showed that Au-NP10 and Au-NP80 induced different patterns of ROS generation with Au-NP10 generating higher levels of ROS than Au-NP80.

The effect of Au-NP10 and Au-NP80 on *p53* mRNA level was analyzed using reverse-transcriptase polymerase chain reaction (PCR) and real-time PCR (Fig. 1C (i, ii)). Western-blot analysis further confirmed the expression of p53 at the protein level (Fig. 1C (iii)). The results showed a substantial increase in the expression of *p53* at mRNA and protein level in Au-NP-treated MCF-7 cells. Au-NP10 induced higher p53 protein expression compared with Au-NP80. The Au-NP10 and Au-NP80 were able to induce differential activation of *p53* at its mRNA level. Au-NP10 induced higher *p53* mRNA expression than Au-NP80. In order to understand the mechanism of this differential regulation of *p53* at its mRNA level, we conducted a time-course analysis of *p53* 2.5 Kb promoter activation in Au-NP10- and Au-NP80-treated MCF-7 cells (Supplementary Fig. S3). Results showed that both Au-NP10 and Au-NP80 induced differential patterns of *p53* 2.5 Kb promoter activity. Au-NP10 induced 1.5 times higher activation of the *p53* promoter than Au-NP80. Since mRNA synthesis is a direct function of the gene-promoter activation, thus it was established that the difference in the *p53* mRNA expression induced by both the Au-NPs was due to differential p53 promoter activity. Further, the activation of *p53* minimal promoter, carrying three p53 DNA binding site (DBS) in *p53* promoter (Supplementary Fig. S4), was analyzed in Au-NP10- and Au-NP80-treated MCF-7 cells. Similar to *p53* 2.5 Kb promoter *p53*, minimal promoter was also differentially activated by both the Au-NPs (Supplementary Fig. S5). These data established that Au-NP10 and Au-NP80 induced differential activation of the *p53* minimal and *p53* full promoter, thus leading to differential mRNA synthesis. The patterns of *p53* promoter activation and ROS synthesis in Au-NP10- and Au-NP80-treated cells were very similar. Hence, we analyzed whether *p53* promoter activation was ROS-dependent. *p53* full promoter activity was observed in Au-NP10- and Au-NP80-treated MCF-7 cells on ROS quenching using N-acetyl-L-cysteine (NAC) (Supplementary Fig. S6). The Au-NP-induced *p53* promoter activation was abolished on ROS quenching (lane 5 & 6). These data delineated the mechanism of differential *p53* mRNA expression in Au-NP10- and Au-NP80-treated cells. The differential ROS patterns induced differential *p53*

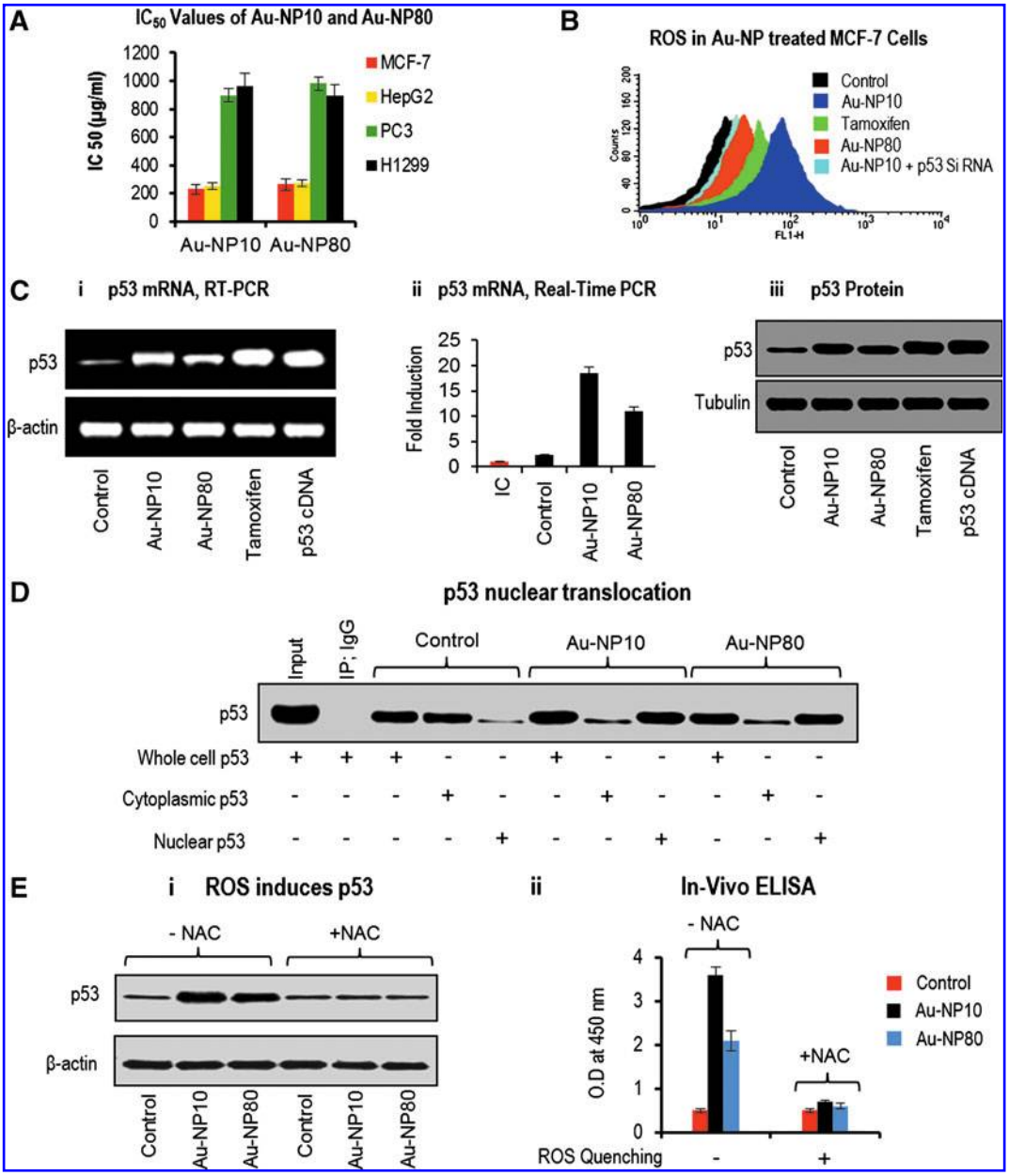

FIG. 1. Au-NP induced p53 gene activation. (A) Au-NPs show cytotoxicity in *p53* + / + cells. IC_{50} values of Au-NP10 and Au-NP80 were determined in MCF-7 (*p53* + / +), HepG2 (*p53* + / +), PC3 (*p53* mutant), and H1299 (*p53* − / −) cells using dimethyl thiazolyl diphenyl tetrazolium salt and lactate dehydrogenase assay. IC_{50} values of Au-NP10 and Au-NP80 in MCF-7 cells were 231 and 263 μg/ml, respectively. HepG2 showed IC_{50} value of 255 and 275 μg/ml on incubation with Au-NP10 and Au-NP80, respectively. The *p53* (mut) PC3 cells showed higher IC_{50} values of 898 and 980 μg/ml on incubation with Au-NP10 and Au-NP80, respectively. Similarly, *p53*-null H1299 cells also showed high IC_{50} values of 964 and 895 μg/ml on incubation with Au-NP10 and Au-NP80, respectively. These IC_{50} values suggested that Au-NP of both sizes were able to induce cytotoxicity in *p53* + / + (MCF-7 and HepG2) cells, whereas PC3 and H1299 cells were resistant to Au-NP mediated cytotoxicity, suggesting that wild-type *p53* may play a crucial role in Au-NP-mediated cytotoxicity. **(B)** The ROS was measured in MCF-7 cells (*black*, control) treated with Au-NP10 (*blue*) and Au-NP80 (*orange*). *p53* silencing abolished Au-NP10 induced ROS (*sky blue*). Tamoxifen was used as positive control (*green*). Au-NP10 induced higher ROS than Au-NP80. **(C)** *p53* expression was analyzed in MCF-7 cells incubated with Au-NP10 and Au-NP80. **(i)** Au-NP10 and Au-NP induced an ~10- and 6-fold increase in p53 mRNA level, respectively, *p53* cDNA transfection serves as positive control, and β-actin is used as loading control. **(ii)** *p53* mRNA was analyzed using real-time PCR. **(iii)** Western blot shows that Au-NP10 and Au-NP80 induced more than a seven- and four-fold increase in p53 level, respectively. *p53* cDNA transfection serves as positive control, and tubulin is used as loading control. **(D)** p53 nuclear translocation was observed in Au-NP-treated MCF-7 cells. The cytoplasmic and nuclear fractions of Au-NP treated MCF-7 cells were collected and were analyzed for p53 protein using immunoprecipitation (IPP). Both Au-NP10 and Au-NP80 were able to induce p53 nuclear translocation, input, and IPP with IgG serving as controls. **(E) (i)** ROS was quenched (with 25-mM NAC) in MCF-7 cells treated with Au-NP10 and Au-NP80. IPP of p53 protein showed that ROS quenching abolished p53 protein expression in Au-NP-treated cells. **(ii)** The p53 ELISA kit also showed that p53 protein was abolished on ROS quenching. IC, internal control; ROS, reactive oxygen species; PCR, polymerase chain reaction; Au-NP, gold nanoparticle. (To see this illustration in color the reader is referred to the web version of this article at www.liebertonline.com/ars).

promoter activity that led to differential *p53* mRNA and protein expression in Au-NP10 and Au-NP80 treated cells. p53 was immunoprecipitated from the nuclear and cytoplasmic fractions of Au-NP10- and Au-NP80-treated MCF-7 cells in order to analyze its nuclear translocation. The results (Fig. 1D) showed that p53 was nuclear (above 90%) in response to Au-NP incubation. The results of p53 immunoprecipitation were repeated through western blotting using β-actin and histone (H3) as cytoplasmic and nuclear loading controls (Supplementary Fig. S7). Since ROS and *p53* are known to regulate each other, the role of ROS in Au-NP10 and Au-NP80-mediated *p53* activation was determined. ROS was quenched using NAC (25 mM) in Au-NP-treated MCF-7 cells. Western blot and *in vivo* enzyme-linked immunosorbent assay (ELISA) showed that Au-NP10 and Au-NP80-mediated increase in p53 protein level was abolished on ROS quenching (Fig. 1E (lane 4–6)). These data established the fact that Au-NP10 and Au-NP80 induced differential ROS patterns in cancer cells, and this Au-NP-induced ROS was instrumental in the upregulation of *p53*.

Au-NP of different sizes induced apoptosis and necrosis in $p53^{+/+}$ *cells*

The role of p53 protein in Au-NP-induced cell death was established as cellular apoptosis, and necrosis was observed in Au-NP10 and Au-NP80 incubated MCF-7 cells, respectively (Fig. 2A). Annexin-V staining showed that Au-NP10 induced apoptosis in MCF-7 (60%; lane 1), whereas Au-NP80 induced cellular necrosis (59%; lane 8). *p53* gene silencing using *p53* siRNA reduced the Au-NP10-mediated apoptosis (lane 6), and Au-NP80 induced necrosis (lane 12), thus establishing the role of *p53* in both the pathways of programmed cell death. The transfection of *p53* cDNA in Au-NP10 and Au-NP80-treated H1299 cells also induced *p53*-mediated apoptosis and necrosis (Supplementary Fig. S8). Caspase-3 and caspase-9 silencing using their respective siRNAs reduced the Au-NP10-induced apoptosis (lane 4 & 5) but showed no effect on the Au-NP80-induced necrosis (lane 10 and 11; Fig. 2A). Further, FAS silencing using FAS siRNA led to no significant change in Au-NP-induced apoptotic and necrotic fractions (lane 3 and 9), suggesting a p53-dependent intrinsic apoptosis in Au-NP-treated cells (Fig. 2A). Terminal deoxynucleotidyl transferase dUTP nick end labeling (TUNEL) assay was used to confirm the fact that Au-NP10 induced cellular apoptosis and Au-NP80 induced cellular necrosis in the cancer cells with *p53* wild-type gene. ELISA-based quantitative TUNEL assay was conducted in the [HCT *p53* (+/+)/HCT *p53* (−/−)], [MCF-7 *p53* (+/+)/MCF-7 *p53* (−/−)], [H1299 *p53* (+/+)/H1299 *p53* (−/−)] and [SAOS-2 *p53* (+/+)/SAOS-2 *p53* (−/−)] cells (Fig. 2B). Results showed that only Au-NP10-treated *p53* (+/+) cells (lanes 1, 3, 5, and 7) showed TUNEL positive staining, and Au-NP80-treated cells were TUNEL negative (red bar). These data again confirmed the fact that Au-NP10 induced apoptosis. In order to differentiate between apoptosis and secondary necrosis/late apoptosis, Au-NP10 and Au-NP80-incubated cells were used for staining with antibodies against single-stranded DNA (ssDNA), as only apoptotic cells generate ssDNA. Au-NP80-treated cells were not positive for staining with MAb against ssDNA, establishing that Au-NP80 induced classical necrosis instead of a secondary necrosis or late apoptosis (Supplementary Fig. S9). The assays for PARP and Caspase 9 cleavage (Fig. 2C) were conducted in Au-NP10- and Au-NP80-treated HCT (*p53*+/+) and HCT (*p53*−/−) cells. Au-NP10 treatment induced PARP and caspase-9 cleavage only in HCT (*p53* +/+) cells, whereas Au-NP80 treatment was

FIG. 2. Au-NP mediated *p53*-dependent apoptosis and necrosis. (A) Au-NP10 induced apoptosis (60%) and Au-NP80 induced necrosis (59%). Au-NP10 and Au-NP80 apoptotic and necrotic fractions were lost on *p53* silencing (lanes 6 and 12), suggesting the role of *p53* in Au-NP-mediated apoptosis and necrosis. The caspase-3 and caspase-9 protein that mediated cellular apoptosis were silenced using their respective siRNAs. Caspase-3 and caspase-9 inhibition abolished cell death only in Au-NP10 treated cells, and Au-NP80-mediated necrosis was not abolished (lanes 4, 5 and 10, 11). To establish the mode of apoptosis (either extrinsic or intrinsic), the FAS receptor was silenced using FAS siRNA in Au-NP incubated MCF-7 cells. FAS silencing led to no difference in the apoptotic or necrotic fractions of Au-NP-treated MCF-7 cells (lanes 3 and 9). These data suggested that Au-NP induced *p53*-dependent intrinsic apoptosis and necrosis. Asterisks signify significant decrease in the apoptotic fraction. **(B)** Au-NP induced cells death was further established using TUNEL assay in [HCT *p53* (+/+)/HCT *p53* (−/−)], [MCF-7 *p53* (+/+)/MCF-7 *p53* (−/−)], [H1299 *p53* (+/+)/H1299 *p53* (−/−)] and [SAOS-2 *p53* (+/+)/SAOS-2 *p53* (−/−)] cells, results showed that onlyAu-NP10-treated cancer cells carrying WT-*p53* gene were TUNEL positive and Au-NP80-treated cells and cells without *p53* gene were TUNEL negative. Asterisks signify significant increase in the TUNEL positive cells. **(C)** Cleavage of the apoptotic marker proteins PARP and caspase-9 was analyzed in Au-NP10- and Au-NP80-treated HCT *p53* (+/+) and HCT *p53* (−/−) cells using western blotting. Au-NP10 induced cleavage of caspase-9 and PARP, but Au-NP80 was unable to induce the cleavage of these apoptotic proteins in HCT *p53* (+/+) cells. In HCT *p53* (−/−) cells, neither Au-NP10 or Au-NP80 treatment was able to induce PARP or caspase cleavage (lane 4–6), β-actin serves as loading control. **(D)** HCT *p53* (+/+) and HCT *p53* (−/−) tumors were grown on the hind leg region of the male nude mice. Both tumors types were treated with Au-NP10 for a period of 4 weeks, and the tumor sizes were frequently measured to study the tumor kinetics **(i)**. Results showed that Au-NP10 induced 72% tumor regression in HCT *p53*(+/+) tumors (*blue line*), whereas no tumor regression was observed in Au-NP10-treated HCT *p53*(−/−) tumors (*red line*). Similarly, HCT *p53* (+/+) and HCT *p53* (−/−) tumors were treated with Au-NP80 for a period of 4 weeks, and the tumor kinetics were observed **(ii)**. Results showed that Au-NP80 induced 71% tumor regression in HCT *p53*(+/+) tumors (*blue line*), whereas no tumor regression was observed in Au-NP10-treated HCT *p53*(−/−) tumors (*red line*). **(E)** Untreated and Au-NP10 and Au-NP80 treated *p53* (+/+) HCT tumors were sectioned to study tissue morphology. Hematoxylin and eosin staining showed organized tissue structure in HCT tumors before treatment; however, Au-NP10 and Au-NP80 treatment led to disintegration of tissue structure, suggesting cell death in the tumor tissue. **(F)** PARP and Caspase-9 cleavage were observed in the Au-NP10 and Au-NP80 treated tumor tissue from the HCT *p53* (+/+) and HCT *p53* (−/−) tumor xenografts. Western blot analysis shows that PARP and Caspase-9 were cleaved only in Au-NP10-treated HCT *p53*(+/+) tumors (lane 2). PARP and caspase-9 cleavage were absent in Au-NP80-treated tumors (lanes 3 and 5) and in HCT *p53* (−/−) tumors, irrespective of the treatment (lane 4–6), β-actin serves as loading control. TUNEL, terminal deoxynucleotidyl transferase dUTP nick end labeling. (To see this illustration in color the reader is referred to the web version of this article at www.liebertonline.com/ars).

unable to induce cleavage of PARP and caspase-9 in both HCT (*p53* + / +) and HCT (*p53* – / –), suggesting a necrotic mode of cell death in Au-NP80-treated cells.

Since the Au-NP10 and Au-NP80 were able to induce apoptosis and necrosis in *p53* (+ / +) cells, we determined whether both Au-NP10 and Au-NP80 were able to induce tumor regression *via* apoptotic and necrotic pathways. HCT (*p53* + / +) and HCT (*p53* – / –) tumors were grown on the hind leg of nude mice. The tumors were treated with Au-NP10 and Au-NP80, respectively, for a period of 4 weeks (Fig. 2D). Results showed that Au-NP10 and Au-NP80 caused 72% and 71% tumor regression, respectively, in the HCT (*p53* + / +) tumors at the end of 4 weeks (Fig. 2D; blue line), whereas no significant change in the tumor volume was observed in HCT (*p53* – / –) tumors (Fig. 2D; red line). Hematoxylin and eosin staining and immuno-histochemical analysis of Au-NP10- and Au-NP80-treated HCT (*p53* – / –) tumors showed that the tumor was dis-integrated on treatment, suggesting cell-death (Fig. 2E). Staining with antip53 PAb421 showed high p53 expression in the nucleus in both Au-NP10 and Au-NP80-treated HCT (*p53* + / +) tumor tissues (Supplementary Fig. S10; upper panel). The Au-NP10-induced apoptosis and Au-NP80-induced necrosis were analyzed in the tumor tissue by staining sections with PAb against ssDNA. Tumors treated with Au-NP10 were positive for staining with PAb against ssDNA, suggesting apoptotic death (Supplementary Fig. S10;

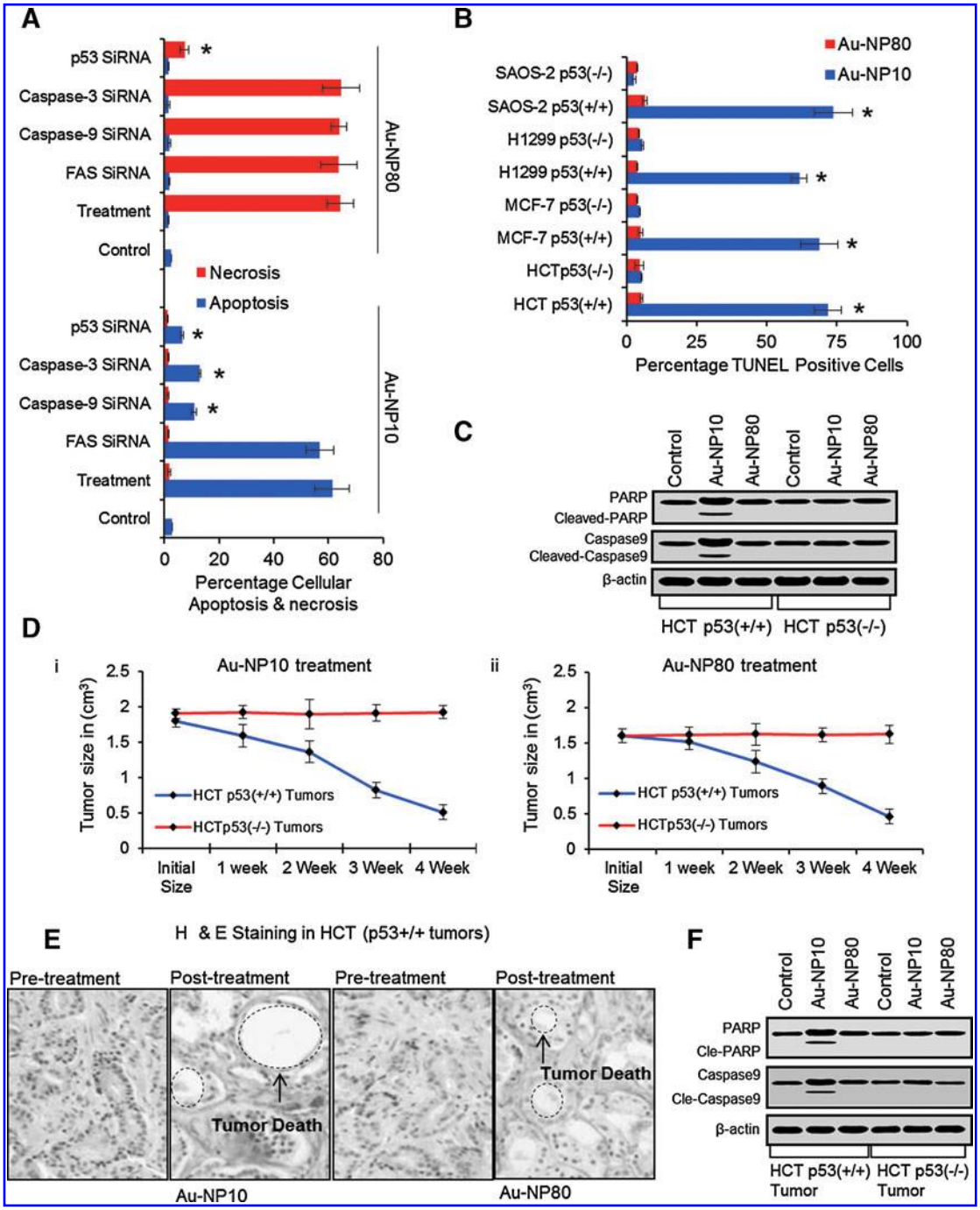

lower panel). On the other hand, Au-NP80-treated tumors did not show staining with Ab against ssDNA, suggesting necrotic death. The cleavage of PARP and caspase-9 was observed in the Au-NP10- and Au-NP80-treated HCT (*p53*+/+) and HCT *p53*(−/−) tumors (Fig. 2F). The results showed that only Au-NP10 induced PARP and caspase-9 cleavage in the HCT (*p53*+/+) tumor tissue, while Au-NP80 did not induce PARP and caspase-9 cleavage. PARP and caspase-9 cleavage was absent in either Au-NP10- or Au-NP80-treated HCT (*p53*−/−) tumor. These data again reconfirm the fact that Au-NPs are cytotoxic toward tumors with wild-type *p53* and Au-NP10 induces p53-dependent apoptosis, whereas Au-NP80 induces *p53*-dependent necrosis.

p53 shows differential post-translational modifications in apoptotic and necrotic cancer cells

The differential activation of *p53* promoter in AuNP10- and AuNP80-treated cells led us to hypothesize that ROS-mediated *p53* activation might be linked to p53 modifications. Since *p53* activation is linked to its post-translational modifications (1, 24, 37), we analyzed the p53 post-translation modification patterns in Au-NP10- and AU-NP80-treated cells. Stress-induced *p53* activation has been shown to involve post-translational modification of p53 *via* phosphorylation, acetylation, and sumoylation (43). Immunoprecipitation results showed that Au-NP10 incubation led to more than a 7-fold increase in p53 phosphorylation and a 6-fold increase in p53 acetylation in MCF-7 cells, whereas Au-NP80 induced a 4-fold increase in p53 phosphorylation and a 3.5-fold increase in p53 acetylation (Fig. 3A (lanes 3–11)); similar results were obtained by *in vivo* ELISA (Supplementary Fig. S11 (i)). ROS quenching using NAC (25 mM) resulted in a significant drop in p53 phosphorylation and acetylation in cells treated with Au-NP10 and Au-NP80 (Fig. 3A (lane 12–18)), (Supplementary Fig. S11 (ii)). Both Au-NP10 and Au-NP80 induced ROS that led to an increase in p53 modifications, making it transcriptionally active.

Earlier reports had shown that p53 activity was dependent on its post-translational modification status. Sequential cassette phosphorylation of p53 has been predicted to produce (19) different regulatory capabilities with regard to gene-expression pattern (6, 31); for example, phosphorylation at specific p53 residues affected its transcriptional activity and/or its selectivity toward a different subset of genes, thus determining the specific type of cellular response to stress (17, 48). We, therefore, analyzed cell extracts for the phosphorylation and acetylation pattern of specific amino acids in p53 that might be responsible for segregation of apoptotic pathway from that of necrosis. The analysis of all p53 Ser, Thr, and Lys residues that undergo phosphorylation and acetylation was conducted through immunoprecipitation using antibodies against phosphorylated $Ser^{6, 9, 15, 20, 33, 37, 46, 315 \text{ and } 392}$, phosphorylated $Thr^{18, 55, 81, 155 \text{ and } 377}$ and acetylated $Lys^{120, 164, 305, 320, 373, 379 \text{ and } 382}$. Untreated MCF-7 cells showed minimal phosphorylation at $Ser^{6, 9, 15}$ and acetylation at $Lys^{379, 382}$ residues of p53 (Fig. 3B). Au-NP10 induced phosphorylation and acetylation at all the known Ser, Thr, and Lys residues (Fig. 3B), whereas Au-NP80 led to a very different pattern of p53 modifications with phosphorylation exclusively at $Ser^{6, 9, 15, 20, 33, 37, 46, 315, 392}$, Thr^{18}, and acetylation at $Lys^{320, 373, 379, 382}$. In addition, phosphorylation was also observed in Ser^{315} (Fig. 3B). *In vivo* ELISA technique also showed similar results to the site specific immunoprecipitation experiments (Fig. 3C (i)–(iii)). These data established that Au-NP10 and Au-NP80 induced differential p53 modifications patterns, thus resulting in differential *p53* transactivation.

The effect of ROS quenching on the phosphorylation and acetylation of all the Ser, Thr, and Lys residues was analyzed. ROS quenching completely abolished the p53 post-translational modification pattern. The phosphorylation and acetylation were minimal at $Ser^{33, 37}$ and were absent at $Ser^{46 \text{ and } 315}$, $Thr^{55, 81, 155, 377}$, and $Lys^{120, 164, 305 \text{ and } 320}$ residues in Au-NP10-treated cells (Fig. 3D), (Fig. 3E (i)). In Au-NP80-treated cells, the pattern was similar to that in Au-NP10-treated cells, except no phosphorylation occurred at $Ser^{33, 37}$ and Lys^{373} (Fig. 3D) and (Fig. 3E (ii)). The results suggested that Au-NP10 induced p53 modifications at the p53 N-terminus, p53 core domain, and p53 C-terminus, whereas Au-NP80 induced p53 modifications only at p53 N- and C-terminus, without any modifications in the core domain. On ROS quenching, the modifications of Ser, Thr, and Lys residues located in and adjacent to the core domain were abolished, thus suggesting that the decision between apoptotic and necrotic cell death might depend on the pattern of p53 post-translational modifications in the core domain. Further, the direct role of phosphorylations at p53 Thr^{55}, Thr^{81}, Thr^{155}, Thr^{155}, and Thr^{377} and acetylation of p53 at Lys^{120}, Lys^{164}, and Lys^{305} in *p53*-dependent apoptosis in Au-NP10-treated MCF-7 and HCT (*p53*+/+) cells was analyzed. *p53* cDNA with mutations at $p53^{\text{Thr55-Ala55, Thr81-Ala81, Thr155-Ala155, The377-Ala377, Lys120-Arg120, Lys164-Arg164, Lys305-Arg305}}$ was constructed. With these mutations, p53 could not be phosphorylated or acetylated at the key amino-acid residues. The mutant p53 was transfected in H1299 and HCT (*p53*−/−) cells, and the cells were treated with Au-NP10 and Au-NP80. The apoptotic and the necrotic fractions of the treated cells were calculated using annexin-V staining. The results showed that in H1299 and HCT cells with MT p53 protein, Au-NP10-indced cellular apoptosis was abolished and instead, a

FIG. 3. p53 post-translational modifications in apoptotic and necrotic cancer cells. (A) ROS induces p53 post-translational modifications. Immunoprecipitation using antiphospho and antiacetylated p53 antibodies showed that both Au-NP10 and Au-NP80 induce p53 phosphorylation and acetylation in MCF-7 cells. Au-NP10 induced higher phosphorylation and acetylation of p53 protein (lane 3–11). ROS quenching using NAC treatment abolished Au-NP10 and Au-NP80-mediated p53 phosphorylation and acetylation (lanes 12–17), input, and IPP with IgG serving as controls. **(B)** p53 phosphorylation and acetylation at $Ser^{6, 9, 15, 20, 33, 37, 46, 315 \text{ and } 392}$, $Thr^{18, 55, 81, 155 \text{ and } 377}$, and $Lys^{120, 164, 305, 320, 373, 379 \text{ and } 382}$ in untreated MCF-7 cells, Au-NP10-treated MCF-7 cells, and Au-NP80-treated MCF-7 cells. **(C) (i–iii)** The results of immunoprecipitation were further confirmed using *in vivo* ELISA. **(D)** p53 phosphorylation and acetylation at the residues just mentioned were analyzed using immunoprecipitation in Au-NP10 treated MCF-7 cells with ROS quenching and Au-NP80 treated MCF-7 cells with ROS quenching. **(E) (i** and **ii)** The results of immunoprecipitation were confirmed using *in vivo* ELISA. ELISA, enzyme-linked immunosorbent assay.

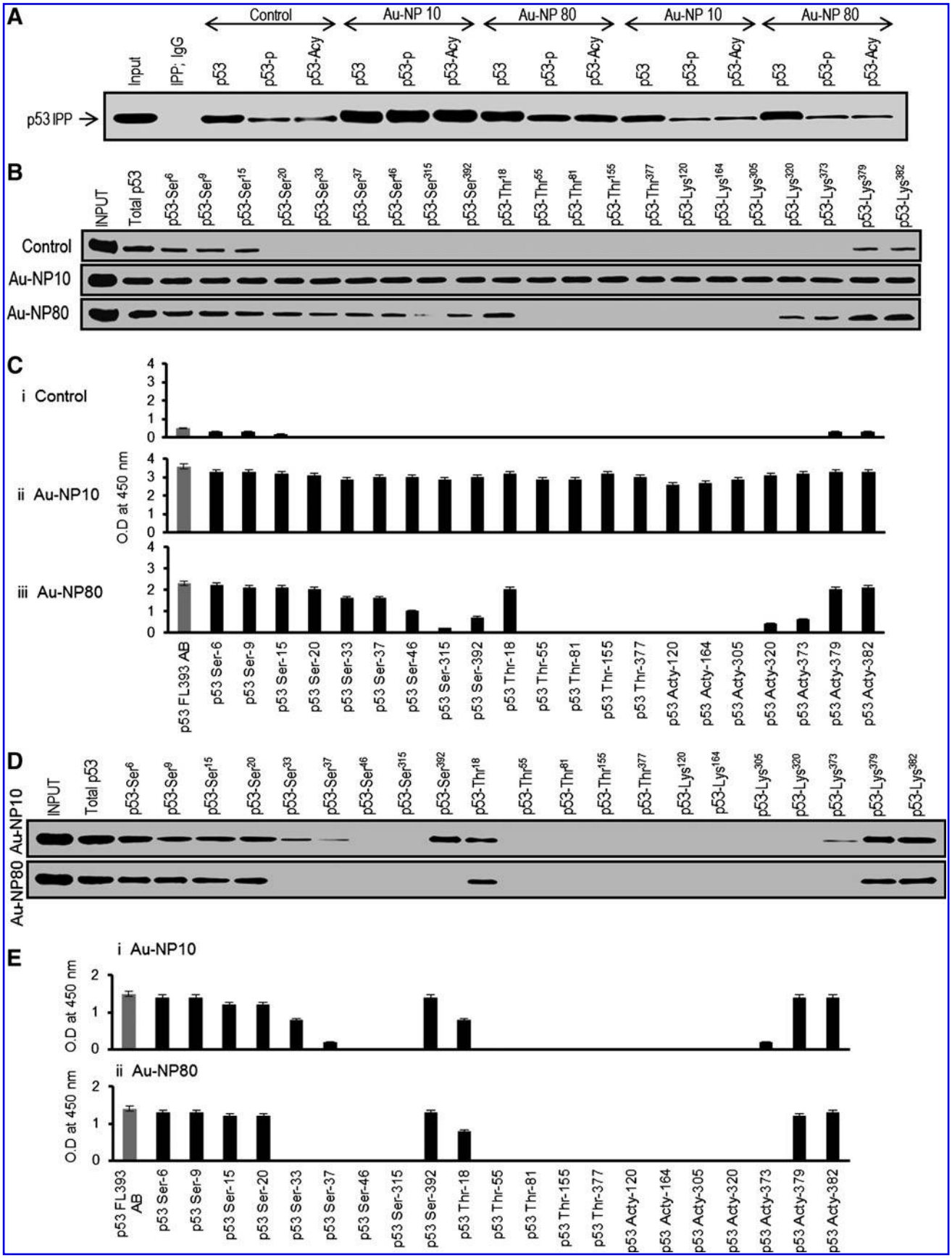
A
Control
Au-NP 10
Au-NP 80
Au-NP 10
Au-NP 80
Input
IPP; IgG
p53
p53-p
p53-Acy
p53 IPP
B
INPUT
Total p53
p53-Ser6
p53-Ser9
p53-Ser15
p53-Ser20
p53-Ser33
p53-Ser37
p53-Ser46
p53-Ser315
p53-Ser392
p53-Thr18
p53-Thr55
p53-Thr81
p53-Thr155
p53-Thr377
p53-Lys120
p53-Lys164
p53-Lys305
p53-Lys320
p53-Lys373
p53-Lys379
p53-Lys382
Control
Au-NP10
Au-NP80
C
i Control
ii Au-NP10
iii Au-NP80
O.D at 450 nm
p53 FL393 AB
p53 Ser-6
p53 Ser-9
p53 Ser-15
p53 Ser-20
p53 Ser-33
p53 Ser-37
p53 Ser-46
p53 Ser-315
p53 Ser-392
p53 Thr-18
p53 Thr-55
p53 Thr-81
p53 Thr-155
p53 Thr-377
p53 Acty-120
p53 Acty-164
p53 Acty-305
p53 Acty-320
p53 Acty-373
p53 Acty-379
p53 Acty-382
D
Au-NP10
Au-NP80
INPUT
Total p53
p53-Ser6
p53-Ser9
p53-Ser15
p53-Ser20
p53-Ser33
p53-Ser37
p53-Ser46
p53-Ser315
p53-Ser392
p53-Thr18
p53-Thr55
p53-Thr81
p53-Thr155
p53-Thr377
p53-Lys120
p53-Lys164
p53-Lys305
p53-Lys320
p53-Lys373
p53-Lys379
p53-Lys382
E
i Au-NP10
ii Au-NP80
O.D at 450 nm
p53 FL393 AB
p53 Ser-6
p53 Ser-9
p53 Ser-15
p53 Ser-20
p53 Ser-33
p53 Ser-37
p53 Ser-46
p53 Ser-315
p53 Ser-392
p53 Thr-18
p53 Thr-55
p53 Thr-81
p53 Thr-155
p53 Thr-377
p53 Acty-120
p53 Acty-164
p53 Acty-305
p53 Acty-320
p53 Acty-373
p53 Acty-379
p53 Acty-382

significant increase in the cellular necrotic fraction was observed (Supplementary Fig. S12; lane 2 and 3). These data confirm that the post-translational modifications of $p53^{Thr55, Thr81, Thr155, Thr155, Thr377, Lys120, Lys164 and Lys305}$ are indispensable for *p53*-mediated apoptosis.

ROS induces different sets of cellular kinases and acetylases in apoptotic and necrotic cancer cells

p53 modification pattern is linked to its trans-activation. Since different levels of ROS activated *p53* differentially, we wanted to determine whether specific sets of kinases and acetylases control p53 modification in response to different sizes of Au-NPs. Since Au-NP10 and Au-NP80 produced differential ROS, we sought to find whether this could result in activation of different p53 interacting cellular kinases and acetylases in controlling p53 modifications. Western blot analysis showed that, in Au-NP10-treated MCF-7 cells, the levels of cellular kinases SPT16, PK2, CAK, JKK2, CSN, CKL-δ, PIK3, ERK2, SAPK4, HIPK2, and JNK2α2 were higher and they interacted with p53 whereas they were absent in Au-NP80-treated cells. However, Au-NP80 induced expression of and interaction with p38, JNK1a1, SSRP1, ATR, cDK2, ERK-1, ATM, cDK1, cK2, cHK2, and DNA-PK (Fig. 4A). In a similar manner, we observed that Au-NP10 and Au-NP80 induced different sets of p53 interacting acetylases (Fig. 4B), while cellular acetylases MOZ, TIF2, HGCNS, hMOF, RIP160, PCAF, and AIB1 were upregulated and interacted with p53 only in Au-NP10-treated cells. On the other hand, p300, CBP, TIP60, and BRPF1 were upregulated by both Au-NP10 and Au-NP80 (Fig. 4B). Results of western blots were rechecked using co-immunoprecipitation between p53 and the various p53-interacting kinases and acetylases (Fig. 4C, D). It was, thus, assumed that different sizes of Au-NP induced activation of different sets of p53-specific acetylases and kinases. ROS might be directly responsible for the activation of p53 interacting kinases and acetylases, as ROS quenching abolished the upregulation of these kinases and acetylases (Fig. 4A: Lanes 4 and 5) and (Fig. 4B: Lanes 4 and 5). The results suggested that the level of ROS might control synthesis of specific sets of kinases and acetylases in response to Au-NP size.

These data revealed a complex pathway of ROS-mediated p53 regulation in MCF-7 cells. Depending on the status of ROS, the cellular kinases and acetylases are activated in these cells, which phosphorylate and acetylate p53 in a predesigned manner. This controlled post-translational modification of p53, regulates its transcriptional activity, and determines the ability of p53 transcription factor to bind to its DBS in the promoter of its downstream genes. This ROS-mediated regulation of p53 phosphorylation and acetylation, through activation of two sets of p53-interacting kinases and acetylases in Au-NP-treated cells, controls the transcriptional status of p53 and, thus, determines the p53-dependent apoptotic or necrotic mode of cell death.

Activated p53 *of different types induced apoptotic and necrotic gene clusters*

The effect of Au-NP-induced p53 post-translational modifications on cellular apoptosis and necrosis was observed in MCF-7 cells. Inhibition of p53 phosphorylation (using serine threonine kinase inhibitors) and acetylation (using *SIRT-1*) reduced Au-NP-mediated apoptosis and necrosis (Supplementary Fig. S13), thus linking the differential post-translational modification of p53 with the transcription of p53 downstream apoptotic and necrotic genes. We analyzed the expression of p53 downstream genes that were responsible for cell death (15) in Au-NP-treated cells by utilizing real-time PCR and *in vivo* ELISA. Interestingly, in MCF-7 cells, Au-NP10 induced expression of 50 p53-regulated genes responsible for p53-mediated apoptosis (Supplementary Table ST1), and Au-NP80 activated a set of 59 necrotic genes involved in cell death (Supplementary Table ST2 and Supplementary Fig. S14). p53 down-stream genes p63, p73, BP1, PUMA, PIG8, p53AIP, FAS, FADD, Caspase-10, Caspase-1, BAX, BAD, and APAF-1 were exclusively induced on Au-NP10 treatment (Fig. 5A). Caspase-8 and NOXA that have been reported to be involved in both apoptosis and necrosis were upregulated in both Au-NP10 and Au-NP80-treated cells. In Au-NP80 treated cells, we observed expression of caspase-14, BIRC7, BRCA2, NOXA, Calpain, CathepsinQ, Clu, Gadd45, and Xrcc3 (Fig. 5B).

Chromatin immunoprecipitation (ChIP), in Au-NP10 and Au-NP80-treated MCF-7 cells, showed that *p53* was involved in up-regulating its down-stream genes p21, *BAX* (apoptotic gene), and *CathepsinQ* (necrotic gene) (18, 40) in inducing apoptosis and necrosis. ChIP analysis showed that p53 showed higher binding at *p215*′-DBS in Au-NP10-treated cells (Fig. 5B (a)). Quantitative ChIP using real-time PCR showed twofold p53 binding on *p215*′-DBS in Au-NP10-treated cells than in Au-NP80-treated cells (Fig. 5C (a)). ChIP on *BAX* promoter (18) showed that Au-NP80-activated p53was unable to bind to the p53 DBS at the *BAX* promoter (Fig. 5B (b); Fig. 5C (b)). By contrast, ChIP on *CathepsinQ* promoter showed that p53 activated by Au-NP10 treatment did not bind to the p53 DBS at the *CathepsinQ* promoter. On the other hand, Au-NP80-activated p53 was bound to p53 DBS at the *CathepsinQ* promoter (Fig. 5B (c); Fig. 5C (c)). This differential binding of p53, by virtue of its differential post-translational modification pattern, to p53 DBS at the respective promoters of the p53 downstream apoptotic and necrotic genes validated our hypothesis that Au-NP of different sizes generated and activated p53 of different types. This established the fact that the differential post-translational modification patterns of p53 induced by Au-NP10 and Au-NP80 incubation were responsible for the difference in the affinity of p53 toward the DBS of its downstream genes involved in apoptosis and necrosis. It could then be inferred that an activated p53 lacking phosphorylation and acetylation at the core domain induced the necrotic gene cluster. These results clearly indicated that similar to apoptosis, necrosis was also regulated tightly by *p53* and was also programmed. The segregated pattern of expression of two different p53-dependent gene clusters leading to apoptosis and necrosis suggested that the post-translational modification of p53 in response to different sizes of Au-NP might have generated two different types of activated *p53*.

Discussion

p53 activates a variety of genes, which, in-turn, trigger cell-cycle arrest and promote apoptosis, differentiation, or senescence (48). In response to a given death stimulus (47, 49), the cell might undergo apoptosis or necrosis depending on the dose of the insult. Necrosis is a passive cellular demise resulting from unmanageable physical damage. We have discovered that small-size Au-NP10 induced *p53*-dependent

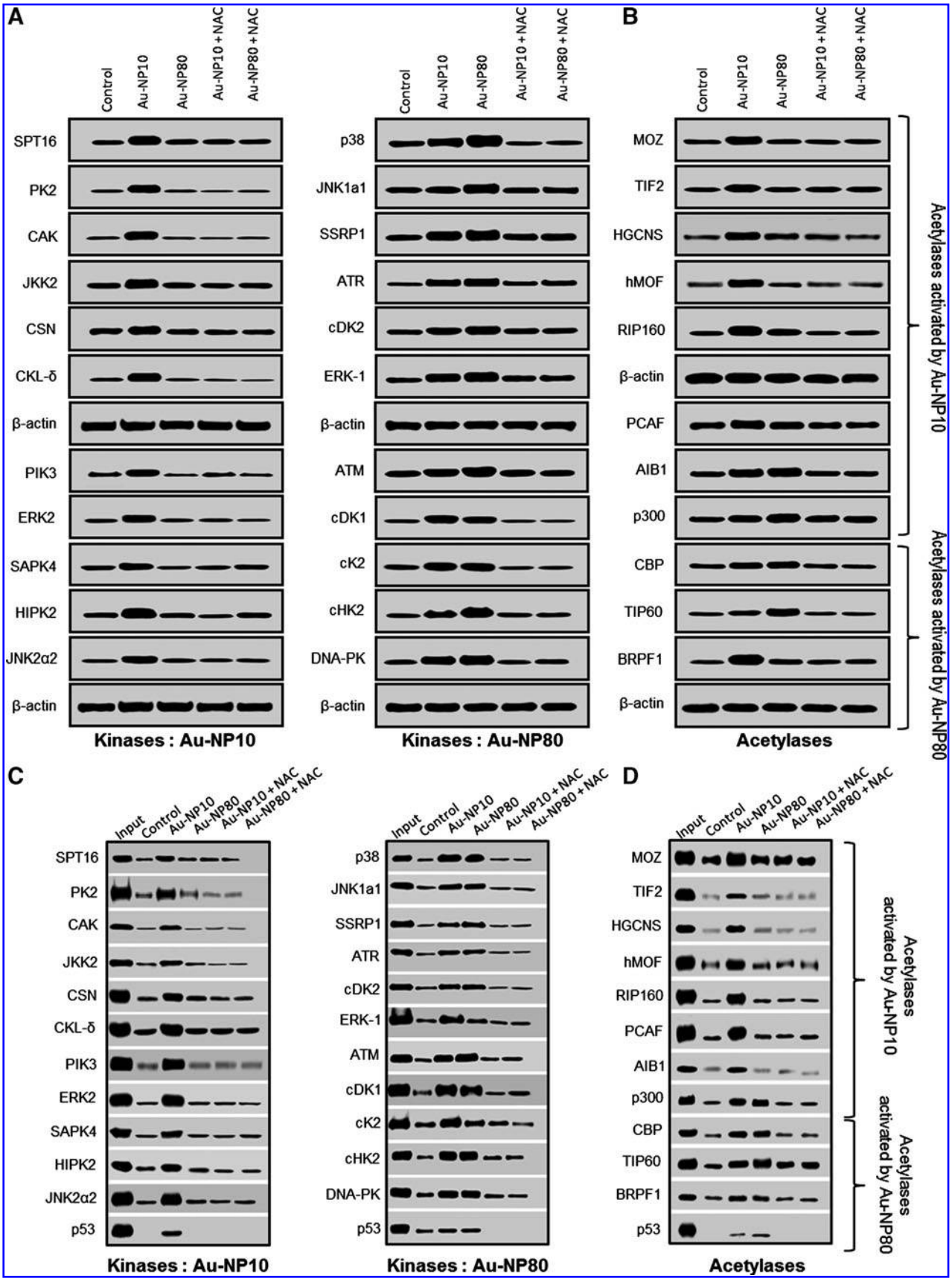

FIG. 4. ROS induced different sets of p53-interacting kinases and acetylases in apoptotic and necrotic cancer cells. (A) Western-blot analysis of p53-interacting kinases in Au-NP10 and Au-NP80 treated MCF-7 cells. **(B)** Western blot analysis of p53-interacting acetylases in Au-NP10 and Au-NP80 treated MCF-7 cells. **(C)** Co-immunoprecipitation using antibodies against activated p53-interacting kinases in Au-NP10 and Au-NP80 treated MCF-7 cells. **(D)** Co-immunoprecipitation using antibodies against activated p53-interacting acetylases in Au-NP10 and Au-NP80-treated MCF-7 cells.

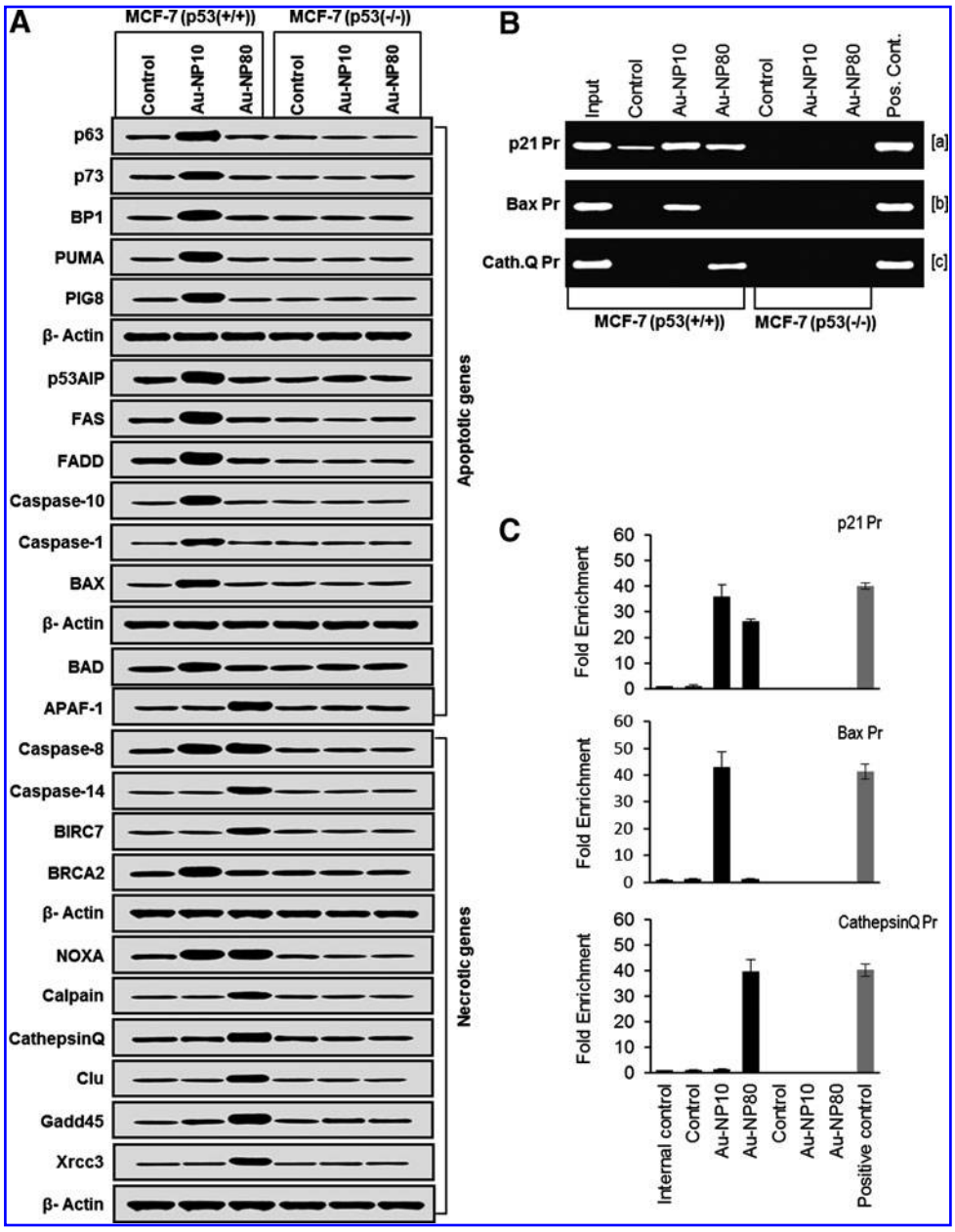

FIG. 5. ***p53*** **downstream apoptotic and necrotic gene clusters. (A)** Western-blot analysis of p53 downstream gene products (involved in p53-mediated cell-death) in Au-NP10 and Au-NP80 incubated MCF-7 *p53* (+/+) and MCF-7 *p53* (−/−) cells. The proteins expressed in Au-NP10-treated MCF-7 p53 (+/+) cells were apoptotic, and the proteins over-expressed in Au-NP80-treated MCF-7 *p53* (+/+) cells were necrotic (lane 1–3). The *p53* downstream apoptotic or necrotic proteins were not up-regulated either on Au-NP10 or on Au-NP80 treatment in MCF-7 *p53* (−/−) cells (lane 4–6). **(B) (a)** Chromatin immunoprecipitation (ChIP) on *p53*-DBS in *p21* promoter in the MCF-7 *p53* (+/+) and MCF-7 *p53* (−/−) cells treated with Au-NP10 and Au-NP80. **(b)** ChIP on p53-DBS in *BAX* promoter in the MCF-7 *p53* (+/+) and MCF-7 *p53* (−/−) cells treated with Au-NP10 and Au-NP80. **(c)** ChIP on p53-DBS in *CathepsinQ* promoter in the MCF-7 *p53* (+/+) and MCF-7 *p53* (−/−) cells treated with Au-NP10 and Au-NP80. The data show that activated p53 in Au-NP-10-treated MCF-7 p53 (+/+) cells binds strongly to *p21* promoter, binds to *BAX* promoter and not to the *CathepsinQ* promoter. p53 activated by Au-NP80 only binds to the p53-DBS in the *CathepsinQ* promoter and not to the *Bax* promoter, suggesting that p53-post-translational modifications determined the binding patterns to promoters of p53 downstream genes. Binding on *p21*, *bax*, or *CathepsinQ* promoters was absent in *p53* null MCF-7 *p53* (−/−) cells (lane 5–7). Input and tamoxifen treatment in MCF-7 *p53* (+/+) cells serves as controls. **(C)** The results of chromatin immunoprecipitation were reconfirmed using real-time ChIP. DBS, DNA binding site.

apoptosis, whereas large-size Au-NP80 induced *p53*-dependent necrosis in cancer cells. Both Au-NP10 and Au-NP80 could regress HCT (*p53*+/+) tumor *via* apoptotic and necrotic pathways, respectively.

We established that *p53*-dependent apoptosis and necrosis are controlled by cellular ROS. Au-NP10 produced a different pattern of ROS production in comparison to Au-NP80, and this differential ROS profile resulted in activation of different sets of p53 interacting cellular kinase and acetylase, which led to differential p53 post-translational modifications. ROS plays multiple roles in tumor initiation, progression, and maintenance. ROS levels were shown to increase in cells exposed to various stress agents including anticancer drugs (5), and they promoted apoptosis by stimulating pro-apoptotic signaling molecules, such as *ASK1*, *JNK*, and *p38* (5). It also played a pivotal role in *p53*-induced apoptosis (5) through activation of mitogen-activated protein kinases (MAPKs), *ERK*s, *JNK*s, and *p38* kinase cascade.

The differential phosphorylation and acetylation of p53 might have generated two distinct forms of activated p53 (directed by the presence or absence of phosphorylation and acetylation on the p53 core-domain). The activated p53 generated by Au-NP10 had higher DNA-binding efficiency, and it switched on 50 apoptotic genes. On the other hand, Au-NP80 activated another form of p53 with a high affinity for p53-DBS of the 59 necrotic genes. We have proposed that the

observed differential pattern of p53 post-translational modifications due to activation of different sets of p53 kinase and acetylase, in response to Au-NP-size dependent stress signals, might be responsible for the expression of differential gene clusters *via p53* activation.

Earlier reports had shown that *p53* activity was dependent on its post-translational modification status. Sequential cassette phosphorylation of p53 has been predicted to produce different regulatory capabilities with regard to gene expression pattern (14); phosphorylation at specific p53 residues affected its transcriptional activity and/or its selectivity toward different subset of genes, thus determining the specific type of cellular response to stress (5, 10). Distinct p53 acetylation cassettes also differentially influenced gene expression and cell fate; specifically, acetylation of $Lys^{373/382}$ resulted in induction of p21 (32) that led to cell-cycle arrest. Since Au-NP10 and Au-NP80 induced differential p53 modifications, it might have stabilized and activated p53 differently, thus allowing it to upregulate different sets of downstream genes. Au-NP10-treated cells induced phosphorylation at $Ser^{6, 9, 15, 20, 33, 37, 46, 315, 392}$, $Thr^{18, 55, 81, 155, 377}$ and acetylation at $Lys^{120, 164, 305, 320, 373, 379, 382}$. On the other hand, Au-NP80 induced phosphorylation at $Ser^{6, 9, 15, 20, 33, 37, 46, 315, 392}$, Thr^{18} and acetylation at $Lys^{320, 373, 379, 382}$ residues.

It could then be inferred that an activated p53 lacking phosphorylation and acetylation at the core domain induced the necrotic gene cluster. In Au-NP-treated cells, sequential as well as simultaneous post-translational modifications were first observed in both N- and C-terminus domains of p53. Our work, thus, corroborated earlier findings that phosphorylation of $Ser^{15, 20, 33, 37 \text{ and } 46}$ and Thr^{18} of the N-terminus promoted p53 stabilization (12) and prevented nuclear export (41) by favoring p53 recruitment in a specific set of promoters. Doxorubicin and etoposide were shown to regulate p53 post-translational modifications *via* phosphorylation of several residues. p53 N-terminus phosphorylation (amino acid 1–39) was shown to be responsible for differential p53 downstream effects (25); p53 Ser^{46} phosphorylation activated apoptotic target genes, and its mutation reduced the ability of *p53* to induce cell-cycle arrest (13). IR or UV induced phosphorylation at $Ser^{6, 15, 29, 33, 37}$ residues (34, 35), acetylation of six lysine residues in the C-terminus (36), and Lys^{164} in the core domain by p300/CBP (38) resulted in enhancement of p53 DBS binding and target gene activation. Induction of *pig3* and *Noxa* was shown to be due to acetylation of p53 at $Lys^{320, 373}$ (5, 38), and acetylation of Lys^{120} (38) was important for activation of pro-apoptotic target genes by p53. Our data revealed that the post-translational modification of p53 core domain was indispensable for *p53*-mediated apoptosis. We also established that the lack of phosphorylation and acetylation in p53 core domain might lead to induction of cell death through a *p53*-dependent necrotic pathway. The acetylation and phosphorylation of the DNA-binding domain has been established as a critical modulator of p53-mediated apoptosis (38) that might bring conformation changes.

In conclusion, we have established that different sizes of Au-NP generate differential p53 activation, thus leading the cell to undergo apoptosis or necrosis. Based on the results, we have proposed a model (Fig. 6) showing how cell stress in response to Au-NPs could generate ROS that could activate different sets of kinases and acetylases. Strikingly, p53 auto-activation at both the transcription and proteome level seems to play an important role in dictating the cell fate. It could, thus, be ascertained that the observed Au-NP10- and Au-NP80-mediated HCT (*p53*+/+) tumor regression is a novel strategy which may find wide application of nano particles in cancer therapy.

Materials and Methods

Gold nanoparticles

The Au-NPs were purchased from British Biocell International, Cardiff, United Kingdom. The Au-NPs were pure in nature, they were not surface functionalized. The data related to the purity, size determination, and characterization of the Au-NPs was provided by the company. The quality of the Au-NPs was certified.

Cell culture

MCF-7, HepG2, RKO, PC3, HCT116, and H1299 were procured from NCCS, Pune, India. These cell lines were maintained in DMEM medium. Media were supplemented with 10% fetal bovine serum. All the transfections were carried out using effectene transfection reagent (Qiagen) according to manufacturer's instructions.

Tumor induction

A 80-μl cell suspension containing 1×10^7 cells was subcutaneously injected into the hind legs of each mice, thus producing two sites of MCF-7 tumor per mouse. Tumor volumes were monitored weekly by caliper measurement of the length, width, and height and were calculated using the formula for a semi-ellipsoid ($4/3\pi r^3/2$). After 3 weeks, mice bearing tumors with volumes averaging approximately 200 mm^3 were randomized for treatment. Due to the variations in tumor take

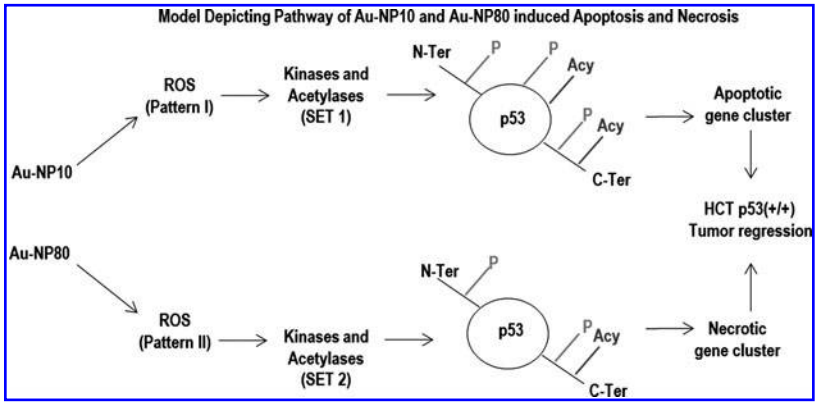

FIG. 6. Mechanism of *p53*-dependent apoptosis and necrosis in cancer cells.

and initial tumor growth as well as the removal of mice for analysis at various time points, the number of mice at each time point varied from experiment to experiment. The number of mice analyzed is reported in the text.

Tissue preparation

All tissues were collected and prepared for pathological examination in a standard manner. Paraffin sections cut at 3 mm were air dried, then placed in a 60°C oven overnight. Sections were de-waxed in xylene, followed by immersion into a solution of 750 ml 30% hydrogen peroxide and 50 ml methanol for 10 min to block endogenous peroxide. Sections were rehydrated to tap water, ready for antigen retrieval. Sections for p53 immunostaining required heat-mediated antigen retrieval treatment. Sections were "superheated" for 4 min in 0.01-M citrate buffer (pH 6.0), then placed in tap water immediately to avoid drying of sections. Sections were transferred to phosphate-buffered saline (PBS) before immunostaining. Immunohistochemistry was performed using a standard avidin-biotin complex. The primary antibody, anti-human p53 was placed on sections at 1:50 dilution for 40 min at room temperature in a wet chamber. Sections were washed in PBS and then incubated in a biotinylated anti-mouse second layer for 30 min. Sections were again washed in PBS, then incubated in the avidin-biotin peroxidase complex (peroxide kit PK6200; Vector Laboratories, Inc.) for 20 min. After three washes in PBS, sections were visualized with activated 3939 di-amino-benzidene-tetra-hydrochloride solution for 10 min, which resulted in a brown end product.

Acknowledgments

The authors acknowledge the support of UPOE (India) and Jawaharlal Nehru University LRE grant for this study.

Author Disclosure Statement

All authors declare no conflict of interest.

References

1. Appella E and Anderson CW. Post-translational modifications and activation of p53 by genotoxic stresses. *Eur J Biochem* 268: 2764–2772, 2001.
2. Bhabra G, Sood A, Fisher B, Cartwright L, Saunders M, Evans WH, Surprenant A, Lopez-Castejon G, Mann S, Davis SA, Hails LA, Ingham E, Verkade P, Lane J, Heesom K, Newson R, and Case CP. Nanoparticles can cause DNA damage across a cellular barrier. *Nat Nanotechnol* 4: 876–883, 2009.
3. Bhattacharya R, Mukherjee P, Xiong Z, Atala A, Soker S, and Mukhopadhyay D. Gold nanoparticles inhibit VEGF165-induced proliferation of HUVEC cells. *Nano Lett* 4: 2479–2481, 2004.
4. Bode AM and Dong Z. Post-translational modification of p53 in tumorigenesis. *Nat Rev Cancer* 4: 793–805, 2004.
5. Bragado P, Armesilla A, Silva A, and Porras A. Apoptosis by cisplatin requires p53 mediated p38alpha MAPK activation through ROS generation. *Apoptosis* 12: 1733–1742, 2007.
6. Chao C, Hergenhahn M, Kaeser MD, Wu Z, Saito S, Iggo R, Hollstein M, Appella E, and Xu Y. Cell type- and promoter-specific roles of Ser18 phosphorylation in regulating p53 responses. *J Biol Chem* 278: 41028–41033, 2003.
7. Cheng Y, C Samia A, Meyers JD, Panagopoulos I, Fei B, and Burda C. Highly efficient drug delivery with gold nanoparticle vectors for *in vivo* photodynamic therapy of cancer. *J Am Chem Soc* 130: 10643–10647, 2008.
8. El-Sayed IH, Huang X, and El-Sayed MA. Surface plasmon resonance scattering and absorption of anti-EGFR antibody conjugated gold nanoparticles in cancer diagnostics: applications in oral cancer. *Nano Lett* 5: 829–834, 2005.
9. El-Sayed IH, Huang X, and El-Sayed MA. Selective laser photo-thermal therapy of epithelial carcinoma using anti-EGFR antibody conjugated gold nanoparticles. *Cancer Lett* 239: 129–135, 2006.
10. Fogal V, Hsieh JK, Royer C, Zhong S, and Lu X. Cell cycle-dependent nuclear retention of p53 by E2F1 requires phosphorylation of p53 at Ser315. *EMBO J* 24: 2768–2782, 2005.
11. Gannon CJ, Patra CR, Bhattacharya R, Mukherjee P, and Curley SA. Intracellular gold nanoparticles enhance non-invasive radiofrequency thermal destruction of human gastrointestinal cancer cells. *J Nanobiotechnol* 6: 2, 2008.
12. Gottifredi V and Prives C. Molecular biology. Getting p53 out of the nucleus. *Science* 292: 1851–1852, 2001.
13. Hao M, Lowy AM, Kapoor M, Deffie A, Liu G, and Lozano G. Mutation of phosphoserine 389 affects p53 function *in vivo*. *J Biol Chem* 271: 29380–29385, 1996.
14. Haupt Y, Rowan S, Shaulian E, Kazaz A, Vousden K, and Oren M. p53 mediated apoptosis in HeLa cells: transcription dependent and independent mechanisms. *Leukemia* 11(Suppl 3): 337–339, 1997.
15. Hoh J, Jin S, Parrado T, Edington J, Levine AJ, and Ott J. The p53MH algorithm and its application in detecting p53-responsive genes. *Proc Natl Acad Sci U S A* 99: 8467–8472, 2002.
16. Jiang W, Kim BY, Rutka JT, and Chan WC. Nanoparticle-mediated cellular response is size-dependent. *Nat Nanotechnol* 3: 145–150, 2008.
17. Jimenez GS, Khan SH, Stommel JM, and Wahl GM. p53 regulation by post-translational modification and nuclear retention in response to diverse stresses. *Oncogene* 18: 7656–7665, 1999.
18. Kaeser MD and Iggo RD. Chromatin immunoprecipitation analysis fails to support the latency model for regulation of p53 DNA binding activity *in vivo*. *Proc Natl Acad Sci U S A* 99: 95–100, 2002.
19. Knights CD, Catania J, Di Giovanni S, Muratoglu S, Perez R, Swartzbeck A, Quong AA, Zhang X, Beerman T, Pestell RG, and Avantaggiati ML. Distinct p53 acetylation cassettes differentially influence gene-expression patterns and cell fate. *J Cell Biol* 173: 533–544, 2006.
20. Li AG, Piluso LG, Cai X, Gadd BJ, Ladurner AG, and Liu X. An acetylation switch in p53 mediates holo-TFIID recruitment. *Mol Cell* 28: 408–421, 2007.
21. Liu B, Chen Y, and St Clair DK. ROS and p53: a versatile partnership. *Free Radic Biol Med* 44: 1529–1535, 2008.
22. Luo J, Su F, Chen D, Shiloh A, and Gu W. Deacetylation of p53 modulates its effect on cell growth and apoptosis. *Nature* 408: 377–381, 2000.
23. Macip S, Igarashi M, Berggren P, Yu J, Lee SW, and Aaronson SA. Influence of induced reactive oxygen species in p53-mediated cell fate decisions. *Mol Cell Biol* 23: 8576–8585, 2003.
24. MacLaine NJ and Hupp TR. How phosphorylation controls p53. *Cell Cycle* 10: 916–921, 2011.
25. Mayo LD, Seo YR, Jackson MW, Smith ML, Rivera Guzman J, Korgaonkar CK, and Donner DB. Phosphorylation of human p53 at serine 46 determines promoter selection and whether apoptosis is attenuated or amplified. *J Biol Chem* 280: 25953–25959, 2005.

26. Mukherjee P, Bhattacharya R, Bone N, Lee YK, Patra CR, Wang S, Lu L, Secreto C, Banerjee PC, Yaszemski MJ, Kay NE, and Mukhopadhyay D. Potential therapeutic application of gold nanoparticles in B-chronic lymphocytic leukemia (BCLL): enhancing apoptosis. *J Nanobiotechnol* 5: 4, 2007.
27. Mukherjee P, Bhattacharya R, Wang P, Wang L, Basu S, Nagy JA, Atala A, Mukhopadhyay D, and Soker S. Antiangiogenic properties of gold nanoparticles. *Clin Cancer Res* 11: 3530–3534, 2005.
28. Oda K, Arakawa H, Tanaka T, Matsuda K, Tanikawa C, Mori T, Nishimori H, Tamai K, Tokino T, Nakamura Y, and Taya Y. p53AIP1, a potential mediator of p53-dependent apoptosis, and its regulation by Ser-46-phosphorylated p53. *Cell* 102: 849–862, 2000.
29. Omata Y, Lewis JB, Lockwood PE, Tseng WY, Messer RL, Bouillaguet S, and Wataha JC. Gold-induced reactive oxygen species (ROS) do not mediate suppression of monocytic mitochondrial or secretory function. *Toxicol In Vitro* 20: 625–633, 2006.
30. Pan Y, Neuss S, Leifert A, Fischler M, Wen F, Simon U, Schmid G, Brandau W, and Jahnen-Dechent W. Size-dependent cytotoxicity of gold nanoparticles. *Small* 3: 1941–1949, 2007.
31. Polley S, Guha S, Roy NS, Kar S, Sakaguchi K, Chuman Y, Swaminathan V, Kundu T, and Roy S. Differential recognition of phosphorylated transactivation domains of p53 by different p300 domains. *J Mol Biol* 376: 8–12, 2008.
32. Saito S, Yamaguchi H, Higashimoto Y, Chao C, Xu Y, Fornace AJ, Jr., Appella E, and Anderson CW. Phosphorylation site interdependence of human p53 post-translational modifications in response to stress. *J Biol Chem* 278: 37536–37544, 2003.
33. Sakaguchi K, Sakamoto H, Lewis MS, Anderson CW, Erickson JW, Appella E, and Xie D. Phosphorylation of serine 392 stabilizes the tetramer formation of tumor suppressor protein p53. *Biochemistry* 36: 10117–10124, 1997.
34. Shieh SY, Ikeda M, Taya Y, and Prives C. DNA damage-induced phosphorylation of p53 alleviates inhibition by MDM2. *Cell* 91: 325–334, 1997.
35. Sykes SM, Mellert HS, Holbert MA, Li K, Marmorstein R, Lane WS, and McMahon SB. Acetylation of the p53 DNA-binding domain regulates apoptosis induction. *Mol Cell* 24: 841–851, 2006.
36. Tang Y, Luo J, Zhang W, and Gu W. Tip60-dependent acetylation of p53 modulates the decision between cell-cycle arrest and apoptosis. *Mol Cell* 24: 827–839, 2006.
37. Tang Y, Zhao W, Chen Y, Zhao Y, and Gu W. Acetylation is indispensable for p53 activation. *Cell* 133: 612–626, 2008.
38. Terui T, Murakami K, Takimoto R, Takahashi M, Takada K, Murakami T, Minami S, Matsunaga T, Takayama T, Kato J, and Niitsu Y. Induction of PIG3 and NOXA through acetylation of p53 at 320 and 373 lysine residues as a mechanism for apoptotic cell death by histone deacetylase inhibitors. *Cancer Res* 63: 8948–8954, 2003.
39. Thomas M and Klibanov AM. Conjugation to gold nanoparticles enhances polyethylenimine's transfer of plasmid DNA into mammalian cells. *Proc Natl Acad Sci U S A* 100: 9138–9143, 2003.
40. Tu HC, Ren D, Wang GX, Chen DY, Westergard TD, Kim H, Sasagawa S, Hsieh JJ, and Cheng EH. The p53-cathepsin axis cooperates with ROS to activate programmed necrotic death upon DNA damage. *Proc Natl Acad Sci U S A* 106: 1093–1098, 2009.
41. Vega FM, Sevilla A, and Lazo PA. p53 Stabilization and accumulation induced by human vaccinia-related kinase 1. *Mol Cell Biol* 24: 10366–10380, 2004.
42. Visaria RK, Griffin RJ, Williams BW, Ebbini ES, Paciotti GF, Song CW, and Bischof JC. Enhancement of tumor thermal therapy using gold nanoparticle-assisted tumor necrosis factor-alpha delivery. *Mol Cancer Ther* 5: 1014–1020, 2006.
43. Vogelstein B, Lane D, and Levine AJ. Surfing the p53 network. *Nature* 408: 307–310, 2000.
44. Vousden KH and Lane DP. p53 in health and disease. *Nat Rev Mol Cell Biol* 8: 275–283, 2007.
45. Vousden KH and Lu X. Live or let die: the cell's response to p53. *Nat Rev Cancer* 2: 594–604, 2002.
46. Xie S, Wang Q, Wu H, Cogswell J, Lu L, Jhanwar-Uniyal M, and Dai W. Reactive oxygen species-induced phosphorylation of p53 on serine 20 is mediated in part by polo-like kinase-3. *J Biol Chem* 276: 36194–36199, 2001.
47. Yuan J, Lipinski M, and Degterev A. Diversity in the mechanisms of neuronal cell death. *Neuron* 40: 401–413, 2003.
48. Zacchi P, Gostissa M, Uchida T, Salvagno C, Avolio F, Volinia S, Ronai Z, Blandino G, Schneider C, and Del Sal G. The prolyl isomerase Pin1 reveals a mechanism to control p53 functions after genotoxic insults. *Nature* 419: 853–857, 2002.
49. Zong WX and Thompson CB. Necrotic death as a cell fate. *Genes Dev* 20: 1–15, 2006.
50. He L, He X, Lim LP, de Stanchina E, Xuang Z, Liang Y, Xue W, Zender L, Magnus J, Ridzon D, Jackson A, *et al.* A micro RNA component of the p53 tumour suppressor network. *Nature* 447: 1130–1134, 2007.

Address correspondence to:
Prof. Uttam Pati
Transcription and Human Biology Laboratory
School of Biotechnology
Jawaharlal Nehru University
New Delhi 110067
India

E-mail: uttam@mail.jnu.ac.in

Date of first submission to ARS Central, June 6, 2011; date of final revised submission, November 4, 2011; date of acceptance, November 4, 2011.

Abbreviations Used

Au-NPs = gold nanoparticles
BD = basal diet
CER I = cytoplasmic extraction reagent I
DBS = DNA binding site
DCFDA = 2′,7′ dichloro-dihydro-fluorescein diacetate
EDTA = ethylenediaminetetraacetic acid
ELISA = enzyme-linked immunosorbent assay
FS = flaxseed diet
IPP = immunoprecipitation
NAC = N-acetyl-L-cysteine
PAGE = polyacrylamide gel electrophoresis
PBS = phosphate-buffered saline
PCR = polymerase chain reaction
ROS = reactive oxygen species
SDS = sodium dodecyl sulfate
ssDNA = single-stranded DNA
TUNEL = terminal deoxynucleotidyl transferase dUTP nick end labeling

This article has been cited by:

1. Pierfausto Seneci. 2012. Small molecules as pro-apoptotic anticancer agents. *Pharmaceutical Patent Analyst* **1**:4, 483-505. [CrossRef]
2. R Gogna, E Madan, P Kuppusamy, U Pati. 2012. Re-oxygenation causes hypoxic tumor regression through restoration of p53 wild-type conformation and post-translational modifications. *Cell Death and Disease* **3**:3, e286. [CrossRef]